C. R. Mecanique 343 (2015) 307–321

Contents lists available at ScienceDirect

Comptes Rendus Mecanique

www.sciencedirect.com

Optimal formation and control of cooperative wheeled mobile robots

Adel Abbaspour [a], Khalil Alipour [b,*], Hadi Zare Jafari [a], S. Ali A. Moosavian [a]

[a] Center of Excellence in Robotics and Control, Advanced Robotics and Automated Systems Lab, Department of Mechanical Engineering, K.N. Toosi University of Technology, 19991 43344, Tehran, Iran
[b] Department of Mechatronics Engineering, Faculty of New Sciences and Technologies, University of Tehran, Tehran, Iran

ARTICLE INFO

Article history:
Received 15 January 2014
Accepted 15 April 2015
Available online 6 May 2015

Keywords:
Wheeled mobile robot
Optimal formation
Automatic control
Numerical methods
Formation control

ABSTRACT

In this paper, the optimal formation of a team of wheeled robot is dealt with for manipulating a common object. The robotic team has been commanded to transport the object from an initial pose along a specified path to a terminal pose. To this end, a proper cost function encompassing various aspects will be established and the grasping points of the object will be then determined employing various numerical optimization techniques such as Simulated Annealing, Genetic Algorithm and Particle Swarm Optimization. Finally, the team is controlled using a virtual structure-based approach and multiple-impedance-control strategy so as the obtained optimal formation can be realized.

1. Introduction

Cooperative multi-robot systems, ranging from multiple mobile robots [1,2], multiple manipulators [3–6], multi-fingered hands [7,8] and multi-legged vehicles [9] have been extensively studied in a variety of contexts. We restrict our attention to cooperative mobile robots that have pivot grasped a common payload. Most publications in formation control of cooperative robots, see, e.g., [2,10–12], classify formation control approaches into three basic strategies, i.e., behavior based, virtual structure, and leader following. Behavior-based approaches start by designing simple behaviors or motion primitives for each individual robot, then more complex motion patterns can be generated by using a weighted sum of the relative importance of these primitives and the interaction of several robots [12]. The main problem of this approach is that the mathematical analysis of this approach is difficult and consequently the convergence of the formation to a desired configuration cannot be guaranteed.

With the leader following strategy, some robots are considered as leaders, while others act as followers. [10]. The leader pursues some group objectives, while the following robots track transformed coordinates of the leader with some prescribed offsets. However, this approach has some disadvantages. Particularly, the chain structure of the approach leads to a poor disturbance rejection property and additionally, the leader's motion is independent of the followers, i.e., there exists no explicit feedback from the followers to the leader. Furthermore, the formation does not tolerate leader faults.

Virtual structures consider the entire formation as a rigid body. The control law for a single vehicle is derived by defining the dynamics of the virtual structure and then translates the motion of the virtual structure into the desired motion of each vehicle. The team motion-planning/control problem now reduces to a well-known single-agent motion planning/con-

* Corresponding author.
E-mail address: k.alipour@ut.ac.ir (K. Alipour).

http://dx.doi.org/10.1016/j.crme.2015.04.003
1631-0721/

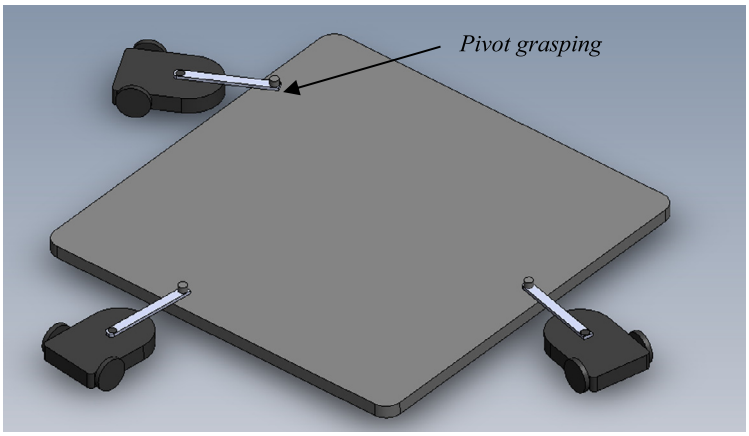

Fig. 1. Several wheeled mobile robots manipulate a large object.

trol problem from which the respective strategies for the individual agents are derived. The formation paradigm has also evolved to allow prescription of parameterized formation maneuvers [13] and group feedback [2,11]. This approach shows the greatest promise for scalability and is a proper method for formation regulation once the desired arrangement of the robotic team is not changing.

Before controlling the robots' formation, the best formation of robots should be found. However, although the problem of formation control has been well studied, finding the best arrangement of robotic members has been less studied [14,15]. As a result, in this paper, this important issue is first addressed. To this end, numerical approaches such as Particle Swarm Optimization (PSO) method and Genetic Algorithm (GA) can be utilized as it has been done in this paper. As in the object manipulation tasks by multiple arms, the formation of the robots does not change, hence a useful formation control approach is virtual structure as it has been utilized in the current work.

In order to control the interaction forces between the robots and payload and hence controlling the desired formation, a control scenario is utilized which, is called Multiple Impedance Control (MIC), [16]. The Multiple Impedance Control (MIC) has been developed for several cooperating arms manipulating a common payload while the internal forces between the arms and payload can also be tuned [17]. The MIC enforces reference impedance on both the manipulator end-points and the manipulated object. This means that both the manipulator end-effectors and the object are controlled to behave like designated impedance in reaction to any disturbing external force on the object.

The organization of this paper is as follows: Section 2 discusses about the dynamics of the system that contains kinematics and dynamics model of a constrained nonholonomic robot and dynamics of an object. In Section 3, a virtual structure method is described to determine the formation of a group of robots. The cost function of a group of robots for payload transportation is derived and then numerical methods are presented to obtain optimum configuration of the robotic team in Section 4. In Section 5, MIC controller is designed to overcome the nature of cooperative interactions between robots and object. In Section 6, a system of three mobile robots with an object is simulated, in which a Remote Center Compliance is attached to each end-effector. The obtained results of computer simulations illustrate the correctness of the suggested method. Finally, Section 7 concludes the paper with a discussion of the results.

2. System dynamics

In this section, the dynamics of a group of wheeled robots that cooperatively manipulate a common object will be derived. To this end, the system is first decomposed into two parts, mainly the robotic members and the manipulated object, and the dynamics of each part is then derived considering the interaction between the robots and the object as it will be described in the next sub-sections.

2.1. Kinematics and dynamics model for a mobile robot in a group

In Fig. 2a, one of the members of a robotic team, which pivotally grasped an object, like that in Fig. 1, has been considered. As it can be observed, a massless solid rod is attached to the robot for manipulation purposes, whose interaction forces due to contact with the object have also been addressed. To model this system, the mobile robot depicted in Fig. 2b is taken into consideration, which is a typical example of a nonholonomic mechanical system. It consists of a vehicle with two driving standard wheels mounted on the same axis, and a front passive wheel. The robot is actuated through two independent DC motors providing the necessary torques for the rear wheels.

The pose of the ith robot in an inertial Cartesian frame $\{X, Y\}$ is completely specified by the vector $\mathbf{q} = [x\, y\, \varphi]^{\mathrm{T}}$, where (x, y) and φ are the coordinates of the point P, and the orientation of the platform with respect to the inertial basis,

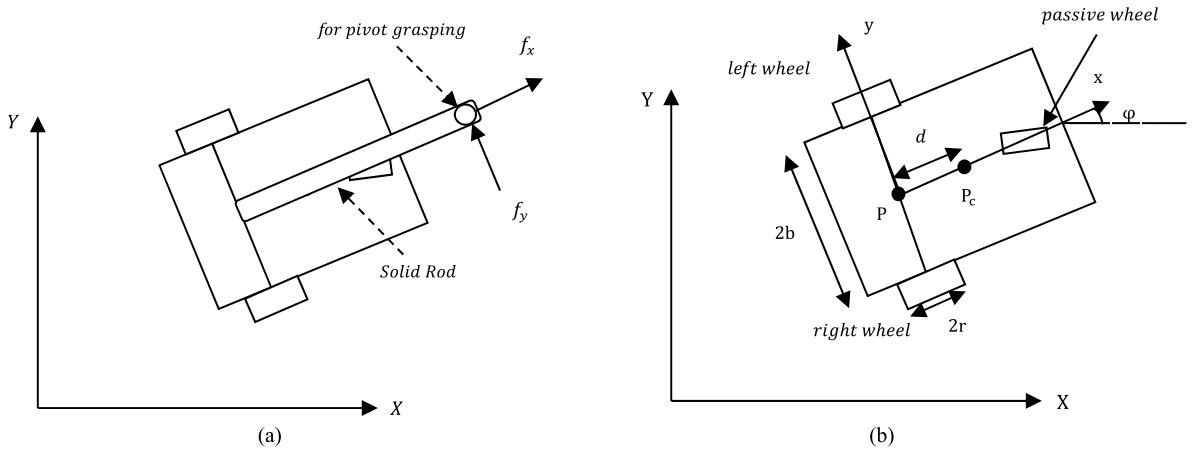

Fig. 2. (a) Nonholonomic mobile robot with attached solid rod for manipulation purposes, (b) Parameters of a nonholonomic mobile robot.

respectively. It is assumed that the robot wheels do not slide. Since the platform is driven by two driving standard wheels that do not slip, then the robot can only move in the direction normal to the axis of the driving wheels, i.e.

$$\dot{x}^{(i)}\sin\left(\varphi^{(i)}\right)-\dot{y}^{(i)}\cos\left(\varphi^{(i)}\right)=0 \tag{1}$$

The above kinematic constraints can be expressed in the form:

$$\mathbf{A}^{(i)}\left(\mathbf{q}^{(i)}\right)\dot{\mathbf{q}}^{(i)}=0 \tag{2}$$

where

$$\mathbf{A}^{(i)}\left(\mathbf{q}^{(i)}\right)=\left[\sin\left(\varphi^{(i)}\right)-\cos\left(\varphi^{(i)}\right)0\right] \tag{3}$$

Additionally the right and left wheels of the robot do not slip and consequently, using kinematic analysis of the robot, the following result can be obtained:

$$\dot{\mathbf{q}}^{(i)}=\mathbf{S}^{(i)}\left(\mathbf{q}^{(i)}\right)\mathbf{v}^{(i)} \tag{4}$$

where $\mathbf{v}=[\dot{\theta}_{\mathrm{r}}\ \dot{\theta}_{\mathrm{L}}]^{\mathrm{T}}$, $\dot{\theta}_{\mathrm{r}}, \dot{\theta}_{\mathrm{L}}$ are the velocities of the right and left wheels respectively. r is the radius of the driving wheel, $2b$ is the distance of two wheels. Also, $\mathbf{S}(\mathbf{q})$ is a 3×2 full-rank matrix as below:

$$\mathbf{S}^{(i)}\left(\mathbf{q}^{(i)}\right)=\begin{bmatrix}\frac{r^{(i)}}{2}\cos(\varphi^{(i)}) & \frac{r^{(i)}}{2}\cos(\varphi^{(i)})\\ \frac{r^{(i)}}{2}\sin(\varphi^{(i)}) & \frac{r^{(i)}}{2}\sin(\varphi^{(i)})\\ \frac{r^{(i)}}{2b^{(i)}} & -\frac{r^{(i)}}{2b^{(i)}}\end{bmatrix} \tag{5}$$

The above matrix is composed of a set of smooth and linearly independent vector fields spanning the null space of $\mathbf{A}(\mathbf{q})$, i.e., $\mathbf{S}^{\mathrm{T}}(\mathbf{q})\mathbf{A}^{\mathrm{T}}(\mathbf{q})=\mathbf{0}$. To derive the dynamics of the ith robot, the Lagrange method is utilized here. To this end, the kinetic energy for the ith robot is first obtained as:

$$\begin{aligned}T^{(i)}=&\frac{1}{2}\left(m_{\mathrm{p}}^{(i)}+2m_{\mathrm{w}}^{(i)}\right)\left(\left(\dot{x}^{(i)}-d^{(i)}\dot{\varphi}^{(i)}\sin\left(\varphi^{(i)}\right)\right)^2+\left(\dot{y}^{(i)}+d^{(i)}\dot{\varphi}^{(i)}\cos\left(\varphi^{(i)}\right)\right)^2\right)\\&+\frac{1}{2}\left(I_{\mathrm{zp}}^{(i)}+2I_{\mathrm{zw}}^{(i)}+2m_{\mathrm{w}}^{(i)}\left(d^{(i)^2}+b^{(i)^2}\right)\right)\dot{\varphi}^{(i)^2}+\frac{1}{2}\left(I_{\mathrm{wy}}^{(i)}\dot{\theta}_{\mathrm{r}}^{(i)^2}\right)+\frac{1}{2}\left(I_{\mathrm{wy}}^{(i)}\dot{\theta}_{\mathrm{L}}^{(i)^2}\right)\\&+2m_{\mathrm{w}}^{(i)}d^{(i)}\dot{\varphi}^{(i)}\left(\dot{x}^{(i)}\sin\left(\varphi^{(i)}\right)-\dot{y}^{(i)}\cos\left(\varphi^{(i)}\right)\right)\end{aligned} \tag{6}$$

where m_{p} and m_{w} are mass of platform and wheels respectively. Besides, I_{zp}, I_{zw} and I_{wy} are the mass moment of inertia of platform about its center of mass in the Z direction, the inertia of each wheel about its center-of-mass in z and y directions, respectively. For the planar robot considered in Fig. 2b, the Lagrange equations can be written as:

$$\frac{\mathrm{d}}{\mathrm{d}t}\frac{\partial T}{\partial\dot{\mathbf{q}}}-\frac{\partial T}{\partial\mathbf{q}}+\mathbf{A}^{\mathrm{T}}(\mathbf{q})\lambda-\boldsymbol{\xi}=\mathbf{0} \tag{7}$$

where $\boldsymbol{\xi}$ is the generalized force vector, λ is the Lagrange multiplier associated with Eq. (1). By substituting Eq. (6) into (7), for the ith robot we can obtain:

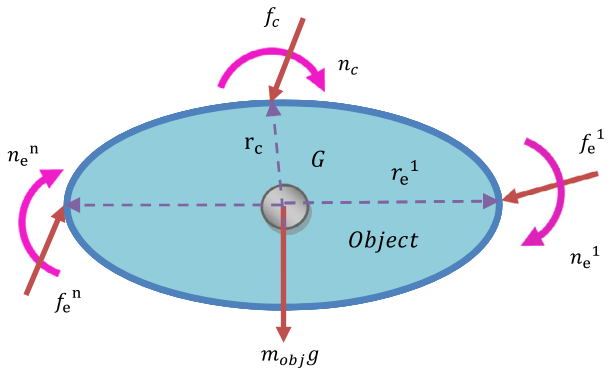

Fig. 3. An object manipulated by cooperating manipulators.

$$\mathbf{M}^{(i)}\left(\mathbf{q}^{(i)}\right)\ddot{\mathbf{q}}^{(i)} + \mathbf{C}^{(i)}\left(\mathbf{q}^{(i)}, \dot{\mathbf{q}}^{(i)}\right) = \mathbf{B}^{(i)}\left(\mathbf{q}^{(i)}\right)\boldsymbol{\tau}^{(i)} + \mathbf{A}^{(i)^{\mathrm{T}}}\left(\mathbf{q}^{(i)}\right)\lambda^{(i)} \tag{8}$$

where $\mathbf{M}(\mathbf{q})$ is a symmetric positive definite mass/inertia matrix and $\mathbf{C}(\mathbf{q}, \dot{\mathbf{q}})$ is the vector of nonlinear velocity-dependent terms. Also, $\mathbf{B}(\mathbf{q})$ is the input transformation matrix and $\boldsymbol{\tau} = [\tau_r\ \tau_l]^{\mathrm{T}}$ is the vector of wheels actuating torques. Substituting Eq. (4) into (8), and then pre-multiplying by $\mathbf{S}^{\mathrm{T}}(\mathbf{q})$, the constraint matrix $\mathbf{A}^{\mathrm{T}}(\mathbf{q})\lambda$ can be eliminated**.** The complete equations of motion of the nonholonomic mobile platform are given by:

$$\bar{\mathbf{M}}^{(i)}\left(\mathbf{q}^{(i)}\right)\dot{\mathbf{v}}^{(i)} + \bar{\mathbf{C}}^{(i)}\left(\mathbf{q}^{(i)}, \dot{\mathbf{q}}^{(i)}\right) = \boldsymbol{\tau}^{(i)} \tag{9}$$

where

$$\bar{\mathbf{M}}(\mathbf{q}) = \mathbf{S}^{\mathrm{T}}\mathbf{M}\mathbf{S}$$
$$\bar{\mathbf{C}}(\mathbf{q}, \dot{\mathbf{q}}) = \mathbf{S}^{\mathrm{T}}\mathbf{M}\dot{\mathbf{S}}\mathbf{v} + \mathbf{S}^{\mathrm{T}}\mathbf{C}$$

Based on Fig. 2a, considering external forces, $\mathbf{F} = \begin{bmatrix} \mathbf{F}_{\mathrm{e}} \\ \mathbf{0} \end{bmatrix}$, $\mathbf{F}_{\mathrm{e}} = \begin{bmatrix} f_x \\ f_y \end{bmatrix}$, indicate force and couple exert on the object by the end-effector of the ith mobile robot, the required torque for moving of each robot can be rewritten as:

$$\bar{\mathbf{M}}^{(i)}\left(\mathbf{q}^{(i)}\right)\dot{\mathbf{v}}^{(i)} + \bar{\mathbf{C}}^{(i)}\left(\mathbf{q}^{(i)}, \dot{\mathbf{q}}^{(i)}\right) + \mathbf{S}^{(i)^{\mathrm{T}}}\mathbf{F}^{(i)} = \boldsymbol{\tau}^{(i)} \tag{10}$$

2.2. Object dynamics

The end-effectors of the physical manipulators are assumed to be pivotally attached to the payload and the locations of the attachment points are fixed with respect to the payload reference frame. By considering the rigid body, as shown in Fig. 3, which is under influence of the torques and forces, the Newton and Euler's equations in the most general case can be written as follows:

$$\mathbf{f}_{\mathrm{c}} + \mathbf{f}_{\mathrm{o}} + \mathbf{f}_{\mathrm{e}}^{(1)} + \cdots + \mathbf{f}_{\mathrm{e}}^{(n)} = m_{\mathrm{obj}}\mathbf{a}_{\mathrm{G}} \tag{11}$$

$$\mathbf{n}_{\mathrm{c}} + \mathbf{n}_{\mathrm{o}} + \mathbf{r}_{\mathrm{c}} \times \mathbf{f}_{\mathrm{c}} + \mathbf{r}_{\mathrm{e}}^{(1)} \times \mathbf{f}_{\mathrm{e}}^{(1)} + \cdots + \mathbf{r}_{\mathrm{e}}^{(n)} \times \mathbf{f}_{\mathrm{e}}^{(n)} + \mathbf{n}_{\mathrm{e}}^{(1)} + \cdots + \mathbf{n}_{\mathrm{e}}^{(n)} = \mathbf{I}_{\mathrm{G}} \times \dot{\boldsymbol{\omega}} + \boldsymbol{\omega} \times \mathbf{I}_{\mathrm{G}}\boldsymbol{\omega} \tag{12}$$

where $\mathbf{f}_{\mathrm{c}}$, $\mathbf{n}_{\mathrm{c}}$ are the forces/torques applied on an acquired object due to contact with the environment. $\mathbf{f}_{\mathrm{e}}^{(i)}$, $\mathbf{n}_{\mathrm{e}}^{(i)}$ are the forces and torques generated by ith robot at the corresponding grasping point, $\mathbf{f}_{\mathrm{o}}, \mathbf{n}_{\mathrm{o}}$ are forces and torques other than contact and end-effector ones applied on an acquired object. m_{obj}, $\mathbf{I}_{\mathrm{G}}$ are mass and mass moment of moment inertia of the object respectively and $\mathbf{r}_{\mathrm{e}}^{(i)}$ is the vector that defines the distance between grasping point and the object center of mass. Now, the above equations can be rewritten in the object attached frame using Euler angles vector which is defined as:

$$\boldsymbol{\omega} = \mathbf{E}\dot{\boldsymbol{\delta}} \tag{13}$$

where matrix $\mathbf{E}$ relates the object's angular velocity and the corresponding Euler angle rates. Substituting Eq. (13) in Eq. (12) yields:

$$\begin{aligned}\mathbf{E}^{\mathrm{T}}\mathbf{I}_{\mathrm{G}}\mathbf{E}\ddot{\boldsymbol{\delta}} + \mathbf{E}^{\mathrm{T}}\mathbf{I}_{\mathrm{G}}\dot{\mathbf{E}}\dot{\boldsymbol{\delta}} + \mathbf{E}^{\mathrm{T}}\boldsymbol{\omega} \times \mathbf{I}_{\mathrm{G}}\boldsymbol{\omega} = {} & \mathbf{E}^{\mathrm{T}}\mathbf{n}_{\mathrm{c}} + \mathbf{E}^{\mathrm{T}}\mathbf{n}_{\mathrm{o}} + \mathbf{E}^{\mathrm{T}}\mathbf{r}_{\mathrm{c}} \times {}^{\mathrm{obj}}_{\mathrm{in}}\mathbf{R}^{\mathrm{in}}\mathbf{f}_{\mathrm{c}} + \mathbf{E}^{\mathrm{T}}\mathbf{r}_{\mathrm{e}}^{\mathbf{1}} \times {}^{\mathrm{obj}}_{\mathrm{in}}\mathbf{R}^{\mathrm{in}}\mathbf{f}_{\mathrm{e}}^{(\mathbf{1})} + \cdots + \mathbf{E}^{\mathrm{T}}\mathbf{r}_{\mathrm{e}}^{(n)} \times {}^{\mathrm{obj}}_{\mathrm{in}}\mathbf{R}^{\mathrm{in}}\mathbf{f}_{\mathrm{e}}^{(n)} \\ & + \mathbf{E}^{\mathrm{T}}\mathbf{n}_{\mathrm{e}}^{(\mathbf{1})} + \cdots + \mathbf{E}^{\mathrm{T}}\mathbf{n}_{\mathrm{e}}^{(n)}\end{aligned} \tag{14}$$

The object equations of motion can be written in matrix form as:

$$\mathbf{M}\ddot{\mathbf{X}} + \mathbf{F}_{\omega} = \mathbf{F}_{\mathrm{c}} + \mathbf{F}_{\mathrm{o}} + \mathbf{G}\mathbf{F}_{\mathrm{e}} \tag{15}$$

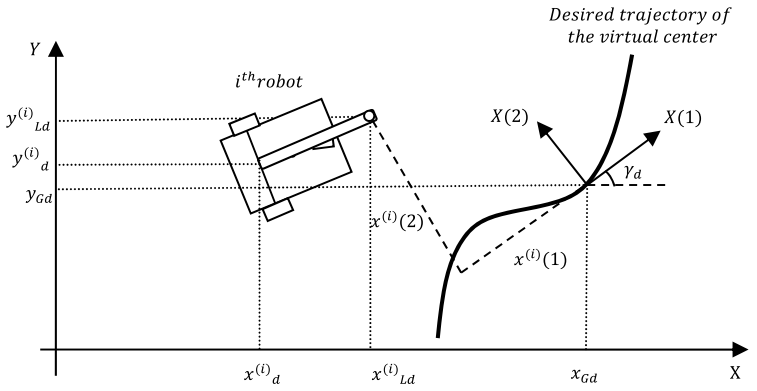

Fig. 4. The virtual structure approach with ith mobile robot.

For a planar system similar to the one depicted in Fig. 1, the $\mathbf{E}$ equals identity matrix, $\mathbf{F}_\omega = \mathbf{F}_o = \mathbf{0}$ and the object angular velocity vector $\boldsymbol{\omega} = \begin{bmatrix} 0 \\ 0 \\ \dot{\gamma} \end{bmatrix}$. Furthermore, other vectors of Eq. (15) can be written as follows:

$$\begin{aligned} \mathbf{X} &= \begin{bmatrix} x_G \\ y_G \\ \gamma \end{bmatrix}_{3\times 1}, \qquad \mathbf{M} = \begin{bmatrix} m_{obj} & 0 & 0 \\ 0 & m_{obj} & 0 \\ 0 & 0 & I_G \end{bmatrix}_{3\times 3} \\ \mathbf{F}_e &= \begin{bmatrix} \mathbf{f}_e^{(1)} \\ \mathbf{f}_e^{(2)} \\ \vdots \\ \mathbf{f}_e^{(n)} \end{bmatrix}_{2n\times 1} \\ \mathbf{G} &= \begin{bmatrix} \mathbf{1}_{2\times 2} & \mathbf{1}_{2\times 2} & \cdots & \mathbf{1}_{2\times 2} \\ \mathrm{A}_1 & \mathrm{A}_2 & \cdots & \mathrm{A}_n \end{bmatrix}_{3\times 2n} \end{aligned} \tag{16}$$

where A_i in the $\mathbf{G}$ matrix means the third row, first and second columns of $[\mathbf{r}_e^{(i)}]^{\times}{}^{obj}_{in}\mathbf{R}$. As a result, the forces needed to be applied on the object by the robots can be determined as follows:

$$\mathbf{F}_e = \mathbf{G}^{\#}(\mathbf{M}\ddot{\mathbf{X}} - \mathbf{F}_c) \tag{17}$$

In Eq. (17), $\mathbf{G}^{\#}$ is the weighted pseudo-inverse of the grasp matrix, which is defined as:

$$\mathbf{G}^{\#} = \mathbf{W}^{-1}\mathbf{G}^{\mathrm{T}}\left(\mathbf{G}\mathbf{W}^{-1}\mathbf{G}^{\mathrm{T}}\right)^{-1} \tag{18}$$

3. Virtual structure method

As it has been previously mentioned, one approach to control the formation of some cooperative robots is the virtual structure method. In this approach it is assumed that the robots are arranged if a virtual structure was being manipulated. For cooperative object manipulation, a formation is generated by the robots because the robots grasp points have fixed distances relative to each other. As a result, for the special case of object manipulation, the real payload is coincident with the virtual structure. Let us consider that the center of the virtual structure is coincident with the center of the payload. For a group of $\underline{n}$ mobile robots, $\underline{n}$ individual reference paths are needed. The reference trajectory of the payload center is described by the coordinates $x_{Gd}(t)$, $y_{Gd}(t)$ in the fixed coordinate frame. Consequently, based on Fig. 4, desired trajectories of the grasp point for individual robots $x_{Ld}^{(i)}(t)$, $y_{Ld}^{(i)}(t)$, $i = 1, \ldots, n$, can describe as:

$$\begin{bmatrix} x_{Ld}^{(i)}(t) \\ y_{Ld}^{(i)}(t) \end{bmatrix} = \begin{bmatrix} x_{Gd}(t) \\ y_{Gd}(t) \end{bmatrix} + \begin{bmatrix} \cos(\gamma_d) & -\sin(\gamma_d) \\ \sin(\gamma_d) & \cos(\gamma_d) \end{bmatrix} \begin{bmatrix} x^{(i)}(1) \\ x^{(i)}(2) \end{bmatrix} \tag{19}$$

where γ_d is the desired orientation of the object along its desired trajectory and $x^{(i)}(1)$, $x^{(i)}(2)$ can possibly be time-varying to allow for time-varying formation shapes. Therefore, $\mathbf{r}_e^{(i)}$ in Eq. (15) can be written as $\mathbf{r}_e^{(i)} = \begin{bmatrix} x^{(i)}(1) \\ x^{(i)}(2) \end{bmatrix}$.

Now, the desired trajectories of each robot $x_d^{(i)}(t)$, $y_d^{(i)}(t)$, $i = 1, \ldots, n$, can be written in terms of the grasping point position as follows:

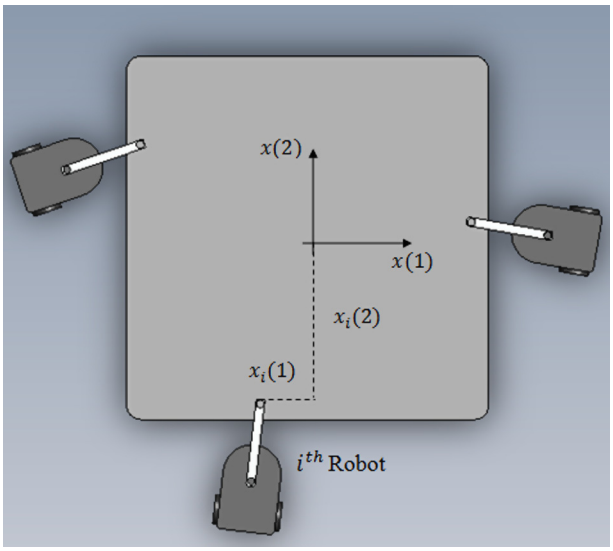

Fig. 5. Object, robot collectives and the parameters that must be optimized.

$$\begin{aligned} x_{\mathrm{d}}^{(i)}(t) &= x_{\mathrm{Ld}}^{(i)}(t) - L^{(i)}\cos\bigl(\varphi_{\mathrm{d}}^{(i)}\bigr) \\ y_{\mathrm{d}}^{(i)}(t) &= y_{\mathrm{Ld}}^{(i)}(t) - L^{(i)}\sin\bigl(\varphi_{\mathrm{d}}^{(i)}\bigr) \end{aligned} \tag{20}$$

where L is the length of the solid rod in each robot. By substitution of Eq. (20) into Eq. (1) leads to:

$$\dot{x}_{\mathrm{Ld}}^{(i)}(t)\sin\bigl(\varphi_{\mathrm{d}}^{(i)}\bigr) - \dot{y}_{\mathrm{Ld}}^{(i)}(t)\cos\bigl(\varphi_{\mathrm{d}}^{(i)}\bigr) + L^{(i)}\dot{\varphi}_{\mathrm{d}}^{(i)} = 0 \tag{21}$$

Using known trajectories of grasping points, i.e. $\dot{x}_{\mathrm{Ld}}^{(i)}(t)$ and $\dot{y}_{\mathrm{Ld}}^{(i)}(t)$, the above first-order differential equation could numerically be solved to find $\varphi_{\mathrm{d}}^{(i)}$. Then using this calculated $\varphi_{\mathrm{d}}^{(i)}$, one can compute $x_{\mathrm{d}}^{(i)}(t)$, $y_{\mathrm{d}}^{(i)}(t)$, $i = 1, \ldots, n$.

For any given path of the object, relative configurations $x^{(i)}(1)$, $x^{(i)}(2)$ induce different motion plans with different performance characteristics, so various selections for the relative configuration of the robots could be possible. Each selection produces a special robots formation. The performance of these different configurations can be evaluated using the considered performance index and cooperative system dynamics. Therefore, dynamics of cooperative object manipulation is used to optimize the relative formation layout, as discussed in the next section.

4. Optimal formation

4.1. Basic concepts

In Fig. 5, a robotic team including $\underline{n}$ nonholonomic mobile robots is considered, which cooperatively transport an object. Each robot member can grasp the object from various points, which generates a special formation. In this section, a strategy for selection of the best grasping points is elaborated, by which the optimal team formation will be found. For the sake of optimality, any performance measure, based on user priorities, can be established. In this research, various important factors such as system energy consumption, load distribution among robots and path smoothness for each robot have been addressed and taken into account as follows.

- **Total consumption energy**

The minimum energy consumption of the robotic team strongly corresponds to the minimum sum of the torques of all robots. Therefore, in Eq. (22) an appropriate criterion of the control effort has been considered.

$$J_{\mathrm{p}} = \int_{t0}^{t_{\mathrm{f}}} \sum_{i=1}^{n} \bigl(\tau_{r_i}^2 + \tau_{L_i}^2\bigr)\mathrm{d}t \tag{22}$$

- **Load distribution**

It is desired that the load is equally distributed among robots to avoid overloading of a special robot. To consider this issue, Eq. (23) is introduced. This index is the sum of ratios of norm of loads handled by each robot:

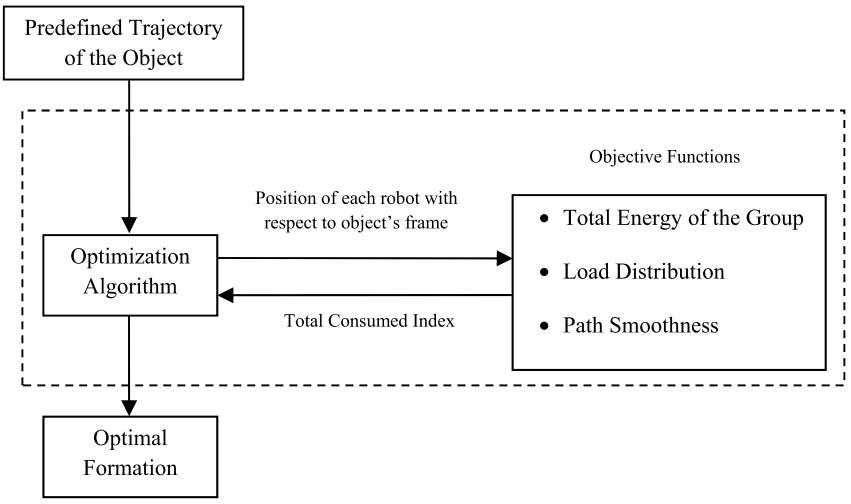

Fig. 6. Basic architecture for finding optimal formation.

$$J_1 = \int_{t_0}^{t_f} \sum_{i=1\neq j}^{n} \sum_{j=1\neq i}^{n} \frac{\|\mathbf{f}_{e_i}\|}{\|\mathbf{f}_{e_j}\|} \mathrm{d}t \tag{23}$$

Note that $\mathbf{f}_{e_i}$ indicate the force affected by ith mobile robot on the payload.

- **Path smoothness**

To address the property of smoothness and change of curvature of the robots path, the curvature effort criterion [18], Eq. (24) has been utilized:

$$J_s = \frac{\sum_{i=1}^{N} \|\Delta K_i\| \Delta S_i}{\rho} \tag{24}$$

where S is the arc length along the robot path, and K denotes the path curvature which can be described as

$$K(s) = \frac{x' y'' - y' x''}{(x'^2 + y'^2)^{3/2}} \tag{25}$$

Additionally, ρ is the distance between initial and final points of the path. To compute J_s, the robot path is divided into N parts. Then, the $\Delta K_i = K_i - K_{i-1}$ and $\Delta S_i = S_i - S_{i-1}$ are calculated, which are the incremental change in curvature and the incremental change in parameter S, respectively.

Now, to consider all of the above issues for optimal formation of the team, one may consider the following relation to describe the final index. The final cost function is a weighted combination of the above-mentioned measures as:

$$J_{\text{total}} = W_p J_p + W_1 J_1 + W_s J_s \tag{26}$$

where W_p, W_1 and W_s are positive weighting factors by which the relative importance of each aspect can adjusted.

The general multi-step architecture for finding the optimal formation is shown in Fig. 6. For each configuration of the robots, the optimization algorithm evaluates the cost function and tries to find the best formation of the group, though the output of the algorithm.

Numerical methods can be employed to find $x^{(i)}(1), x^{(i)}(2);\ i = 1, 2, \ldots, n$ such that the above cost function be minimized. As the dimension of the object is limited and the numerical algorithm should not converge to unacceptable values, the search space is bounded within $x^{(i)}(1) \in [-C_{\max}, C_{\max}]$ and $x^{(i)}(2) \in [-D_{\max}, D_{\max}]$, where $C_{\max}$ and $D_{\max}$ are the maximum possible dimension of the object. In addition, the desired distances $x^{(i)}(1), x^{(i)}(2);\ i = 1, 2, \ldots, n$ should be regulated such that there is no collision between robots. To apply these constraints, numerical values that are out of the desired range are penalized with a high magnitude of objective function. So the improper values are not chosen by the numerical optimization algorithm.

4.2. Employed optimization methods

To solve each optimization problem, numerical solution methods are powerful tools for solving linear and, especially, nonlinear problems; however, the best method is not definite. As a matter of fact, the appropriate method for optimization

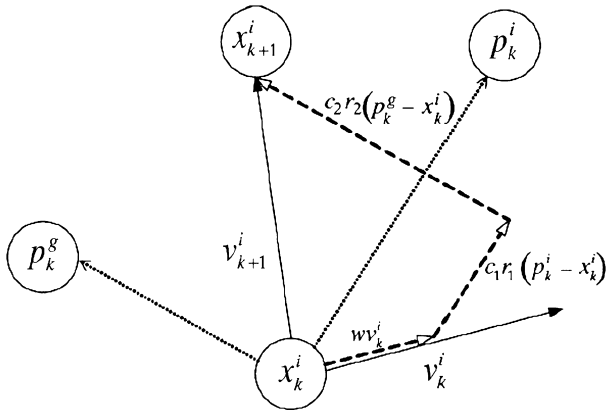

Fig. 7. Schematic of PSO particle value and change rate updating.

can be found by comparison between several numerical algorithms for each problem. Consequently, in this research, three numerical optimization algorithms (PSO, GA and SA) are exploited to find the best optimal formation.

- **Particle Swarm Optimization (PSO)**

PSO method is inspired by the observations of birds flocking and fish schooling. Kennedy and Eberhart [19] proposed this algorithm, which is based on the premise that social sharing of information among members of a species offers an evolutionary advantage. PSO is well suited to handle non-linear, non-convex design spaces with discontinuities and it is robust. It can easily handle continuous, discrete and integer variable types. Comparison of robust optimization methods reveals that PSO is more efficient, and requires fewer number of function evaluations, while leading to a better or the same quality of results. The PSO method does not require specific domain knowledge information, internal transformation of variables or other manipulations to handle constraints. Each particle in PSO has two main characteristics: its value and its change rate. The value of each particle is updated based on the social behavior of the population, which is named swarm. Note that here the word *swarm* is a numerical term related to the PSO method and does not refer to the agents of the multi agent system. According to Kennedy and Eberhart [19], the PSO algorithm can be described as:

$$\begin{aligned} V_i^{k+1} &= wV_i^k + c_1 r_1 \left(P_i^k - X_i^k\right) + c_2 r_2 \left(P_g^k - X_i^k\right) \\ X_i^{k+1} &= X_i^k + V_i^{k+1} \end{aligned} \tag{27}$$

where c_1 (cognitive parameter) and c_2 (social parameter) are positive constants, r_1 and r_2 are two scalar random functions within $[0, 1]$. X_i represents the value of the ith particle in search space; P_i represents the best previous value of the ith particle. P_g Corresponds to the global best particle value in the swarm up to iteration k. V_i represents the change rate of the ith particle and w is the inertia weight. PSO particle value and change rate updating are shown in Fig. 7.

- **Genetic Algorithm**

Genetic Algorithm (GA) is a solution for optimizing problems based on the principle of natural selection "survival of the fittest" that are used successfully in optimization problems. GA is generally able to find good solutions in a reasonable amount of time. When implementing the GAs, the operator needs to choose the suitable parameter settings to ensure the success of the algorithm with high performance and low computational costs simultaneously.

Genetic Algorithm raises a couple of important features. First, it is a stochastic algorithm; randomness as an essential role in genetic algorithms for avoidance of getting trapped in local minimum points. Both selection and reproduction needs random procedures. A second important point is that genetic algorithms always consider a population of solutions. Keeping in memory more than a single solution at each iteration offers a lot of advantages.

- **Simulated annealing**

Simulated annealing is an algorithm for optimizing problems based on emulating physical process. The concept is based on the manner in which liquids freeze or metals recrystallize in the process of annealing. In an annealing process, a melt, initially at high temperature and disordered, is slowly cooled so that the system at any time is approximately in thermodynamic equilibrium. As cooling proceeds, the system becomes more ordered and approaches a "frozen" ground state at $T = 0$. Hence the process can be thought of as an adiabatic approach to the lowest energy state. If the initial temperature of the

system is too low or cooling is done insufficiently slowly, the system may become quenched forming defects or freezing out in metastable states (i.e. trapped in a local minimum energy state) [20,21].

5. Multiple impedance control law

To manipulate an object with several cooperating manipulators, the Multiple Impedance Control (MIC) is a model-based algorithm that enforces designated impedance on all cooperating manipulators and the manipulated object. This algorithm can be used to tune the internal forces between the payload and the robots and is stable even in the presence of mechanical flexibility in the system and hence can be considered as an effective candidate for formation control during object manipulation tasks. The MIC enforces the same reference impedance on both the robot and the manipulated object. This means that both the robot and the object are controlled to behave like a designated impedance in reaction to any disturbing external force on the object. Hence, an accordant motion of the robot and payload is achieved. Based on MIC law, the required controlling force for each robot can be written as

$$\mathbf{Q}_{\text{app}}^{(i)} = \mathbf{Q}_{\text{m}}^{(i)} + \mathbf{Q}_{\text{F}}^{(i)} \tag{28}$$

where $\mathbf{Q}_{\text{m}}^{(i)}$ is the applied control force causing the motion of the ith robot, while $\mathbf{Q}_{\text{F}}^{(i)}$ is the required force to compensate the reaction load effects exerted on the ith robot due to the interaction of the robot and the grasped payload. Additionally, based on MIC approach, a desired impedance law for the object motion is considered as:

$$\mathbf{M}_{\text{deso}}^{(i)}\ddot{\mathbf{e}}_{\text{o}}^{(i)} + \mathbf{K}_{\text{do}}^{(i)}\dot{\mathbf{e}}_{\text{o}}^{(i)} + \mathbf{K}_{\text{po}}^{(i)}\mathbf{e}_{\text{o}}^{(i)} = -\mathbf{F}_c \tag{29}$$

where $\mathbf{e}_{\text{o}} = \mathbf{X}_{\text{des}} - \mathbf{X}$ describes the object tracking error, $\mathbf{K}_{\text{po}}$ and $\mathbf{K}_{\text{do}}$ are control gain matrices, and $\mathbf{M}_{\text{deso}}$ is the object desired mass matrix. By direct comparison of Eqs. (29) and (15), the desired impedance behavior for the ith can be obtained if:

$$\mathbf{F}_{\text{e}_{\text{req}}}^{(i)} = \mathbf{G}^{\#}\left\{\mathbf{M}^{(i)}\mathbf{M}_{\text{deso}}^{-\mathbf{1}(i)}\left(\mathbf{M}_{\text{deso}}^{(i)}\ddot{\mathbf{X}}_{\text{des}}^{(i)} + \mathbf{K}_{\text{do}}^{(i)}\dot{\mathbf{e}}_{\text{o}}^{(i)} + \mathbf{K}_{\text{po}}^{(i)}\mathbf{e}_{\text{o}}^{(i)} + \mathbf{F}_{\text{c}}\right) - \mathbf{F}_{\text{c}}\right\} \tag{30}$$

Therefore, applying the required end-effector forces/torques on the object results in the targeted impedance relationship as described in Eq. (29). As a result, the force-concerned part of the controlling force can be calculated as:

$$\mathbf{Q}_{\text{F}}^{(i)} = \mathbf{S}^{(i)^{\mathbf{T}}}\mathbf{F}_{\text{e}_{\text{req}}}^{(i)} \tag{31}$$

Next, to complete the computation of the controlling force $\mathbf{Q}_{\text{app}}$ as described in Eq. (28), an expression for $\mathbf{Q}_{\text{m}}$ must be obtained. To impose the same impedance law on the mobile robot motion, manipulators, and the object, the impedance law for the ith mobile robot group is written as:

$$\mathbf{M}_{\text{desr}}^{(i)}\ddot{\mathbf{e}}_{\text{r}}^{(i)} + \mathbf{K}_{\text{dr}}^{(i)}\dot{\mathbf{e}}_{\text{r}}^{(i)} + \mathbf{K}_{\text{pr}}^{(i)}\mathbf{e}_{\text{r}}^{(i)} = -\mathbf{F}_c \tag{32}$$

where $\mathbf{e}_{\text{r}} = \mathbf{q}_{\text{des}} - \mathbf{q}$ describes the robot tracking error, $\mathbf{K}_{\text{pr}}$ and $\mathbf{K}_{\text{dr}}$ are control gain matrices, and $\mathbf{M}_{\text{desr}}$ is the robot desired mass matrix. Based on a feedback linearization scheme, the motion-concerned part of the applied torques for ith mobile robot is as follows:

$$\mathbf{Q}_{\text{m}}^{(i)} = \mathbf{S}^{(i)^{\text{T}}}\mathbf{M}^{(i)}\left(\mathbf{q}^{(i)}\right)\mathbf{M}_{\text{desr}}^{-\mathbf{1}(i)}\left[\mathbf{M}_{\text{desr}}^{(i)}\left(\ddot{\mathbf{q}}_{\mathbf{d}}^{(i)}\right) + \mathbf{K}_{\text{dr}}^{(i)}\dot{\mathbf{e}}_{\text{r}}^{(i)} + \mathbf{K}_{\text{pr}}^{(i)}\mathbf{e}_{\text{r}}^{(i)} + \mathbf{F}_{\text{c}}\right] + \mathbf{S}^{(i)^{\text{T}}}\mathbf{C}^{(i)}\left(\mathbf{q}^{(i)}, \dot{\mathbf{q}}^{(i)}\right) \tag{33}$$

The desired trajectory for the system controlled variables, $\mathbf{q}_{\text{des}}$, can be defined based on the desired trajectory for the object motion, $\mathbf{X}_{\text{des}}$, and the grasp condition which was described in Eq. (19).

6. Case studies

6.1. System description

For computer simulation purposes, three wheeled robots have been considered for cooperative object manipulation. The Remote Center Compliance (RCC), Fig. 8, is attached to the whole end-effectors to consider the practical issues (for more details see Ref. [22]). The object has been grabbed with a pivoted grasp condition, i.e. no torque can be exerted on the object by the end-effectors. The task is to move a large and heavy object based on a given desired trajectory. For the system depicted in Fig. 8, the geometric parameters and mass properties are displayed in Tables 1 and 2. The object is initially positioned at $x_{\text{G}} = -0.25$, $y_{\text{G}} = 0$ with $\gamma = 0$, while the initial desired pose is located at $x_{\text{Gd}} = 0$, $y_{\text{Gd}} = 0$ with $\gamma_{\text{d}} = 0$ and it is desired to move towards the goal point within 80 seconds with final $\gamma_{\text{d}} = 90^\circ$ along a smooth path as:

$$\begin{aligned} x_{\text{Gd}} &= \left(7.5\cos(0.04t) - 2.5\cos(0.08t) - \cos(0.12t) - \cos(0.16t) - 2.5\right) \\ y_{\text{Gd}} &= 8\sin^3(0.04t) \\ \gamma_{\text{d}}(t) &= a_0 + a_1 t + a_2 t^2 + a_3 t^3 + a_4 t^4 + a_5 t^5 \end{aligned} \tag{34}$$

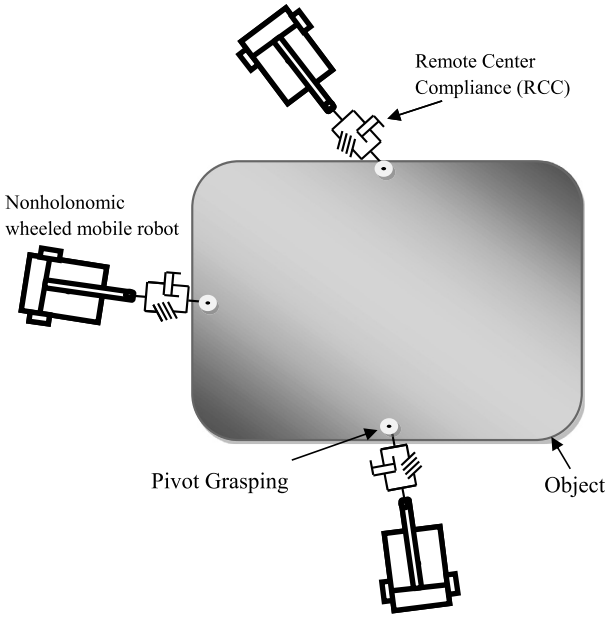

Fig. 8. Three-wheeled mobile robots manipulate a large object.

Table 1
Object properties.

Object mass [kg]	Object mass moment of inertia [kg·m^2]	Length [m]	Width [m]
100	120	3	1

Table 2
Properties of the mobile robot.

Distance from P to P_c	$d = 0.2$ [m]	Mass of wheel	$m_w = 0.82$ [kg]
Distance from wheel to P	$b = 0.3$ [m]	Mass of platform	$M = 70$ [kg]
Radius of wheel	$r = 0.1$ [m]	Platform mass moment of inertia	$I_Z = 6.12$ kg·m^2

Table 3
Position of the robots with respect to object's frame (PSO).

Robot	$x_i(1)$ [m]	$x_i(2)$ [m]
Robot 1	−1.5	0.5
Robot 2	1.5	0.1718
Robot 3	−0.093	−0.5

The desired path for the orientation of the object is a quantic polynomial trajectory. The six constant coefficients $a_0, a_1, a_2, a_3, a_4, a_5$ are constants that can be determined based on desired initial and final conditions and the time duration needed for the path travel [23].

6.2. Obtained results

For the desired trajectory of the object in Eq. (34), the best formation for each robot is obtained employing the suggested strategies using PSO, GA and SA methods, whose results have been summarized in Tables 3, 4 and 5, respectively. The position for each robot is obtained with respect to the object attached coordinate frame. Also the optimized cost function value and elapsed time for these numerical methods is shown in Table 6.

In this case study, the response of the considered robotic group is examined using MIC law. The RCC module is attached to the end-effectors, Fig. 8, to consider practical aspects [23]. Furthermore, for including the effects of model uncertainty, the parameters of the robots are considered to be different in controller and system model. To this end, the mass/inertia matrix of the robot is perturbed by about 20%. In this case, the controller gains are chosen so that the closed-loop system exhibits a critical damping behavior

$$\mathbf{K}_{pr} = 15, \quad \mathbf{K}_{dr} = 20, \quad \mathbf{M}_{desr} = 1, \quad \mathbf{K}_{po} = 5, \quad \mathbf{K}_{do} = 10, \quad \mathbf{M}_{deso} = 1 \quad \text{and} \quad \mathbf{K}_S = 200, \quad \mathbf{K}_D = 500$$

Table 4
Position of the robots with respect to object's frame (GA).

Robot	$x_i(1)$ [m]	$x_i(2)$ [m]
Robot 1	0.6127	0.5226
Robot 2	−0.2312	−0.4999
Robot 3	−0.522	0.2135

Table 5
Position of the robots with respect to object's frame (SA).

Robot	$x_i(1)$ [m]	$x_i(2)$ [m]
Robot 1	−1.342	−0.248
Robot 2	1.325	0.424
Robot 3	1.5	−0.639

Table 6
Optimized cost function value versus analyzed time.

Method	Cost function	Time [s]
PSO	9025.3	245
SA	9536.2	210
GA	9243.6	106

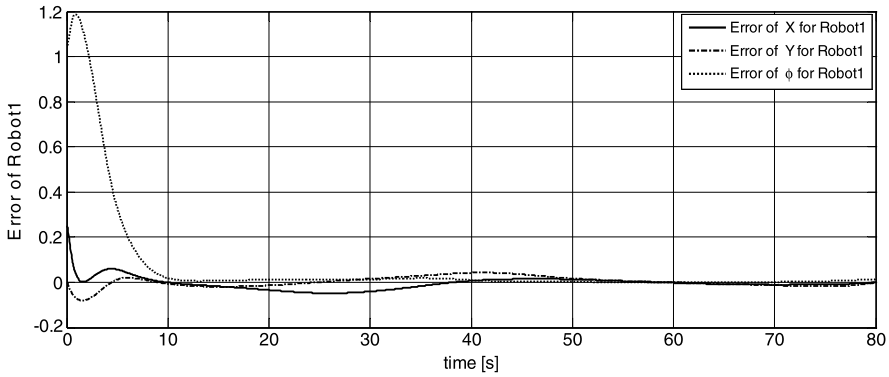

Fig. 9. Errors of robot 1.

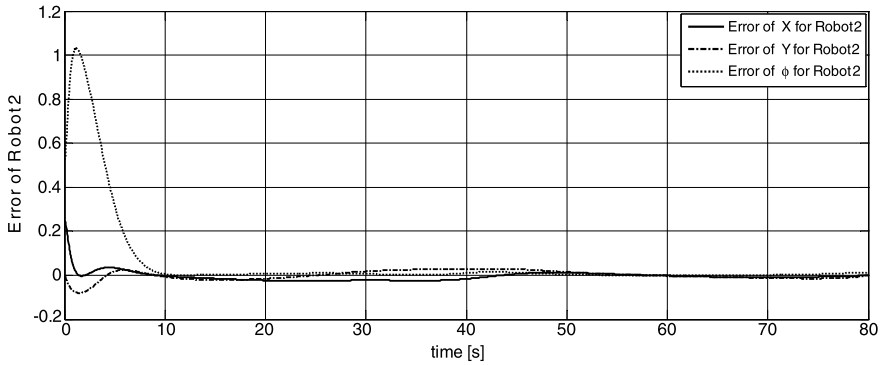

Fig. 10. Errors of robot 2.

where $\mathbf{K}_S$ and $\mathbf{K}_D$ are the spring and damper coefficient of RCC and it is assumed that the RCC unit is initially free of tension or compression. Furthermore, comparing the numerical optimization results, it can be found that PSO presented the lowest amount of the considered cost function. Hence, the initial position for each robot is arranged based on PSO results, which is as follows:

$$\text{Robot 1}: \; x_{c_1} = -1.75, \qquad y_{c_1} = 0.5, \qquad \varphi_1 = \frac{\pi}{4}$$

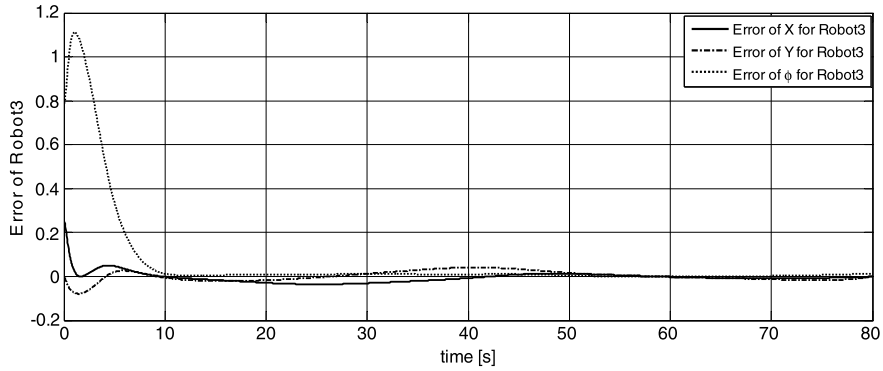

Fig. 11. Errors of robot 3.

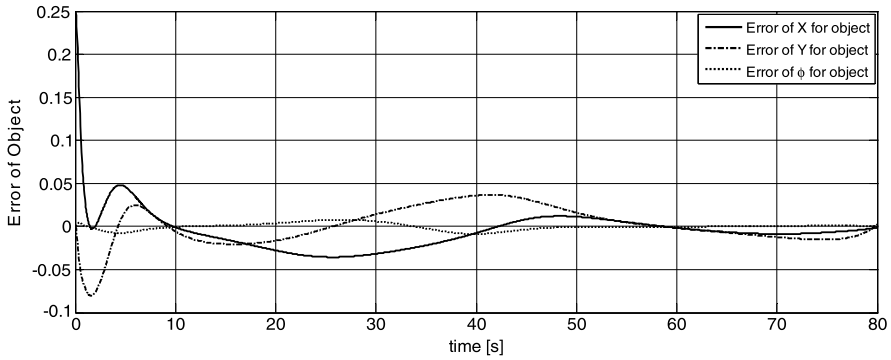

Fig. 12. Errors of object.

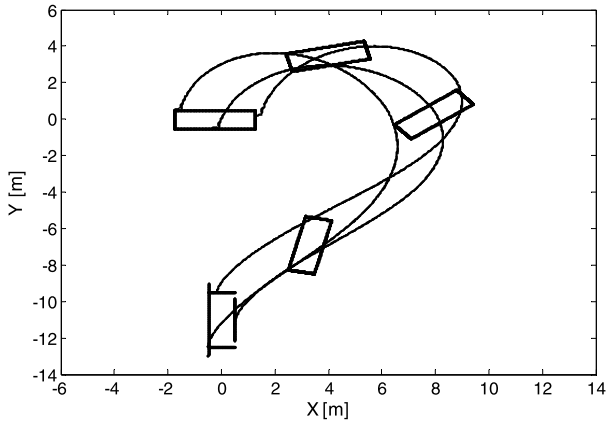

Fig. 13. Desired and real paths of the three robots along with the object pose.

$$\text{Robot 2}: \; x_{c_2} = 1.25, \qquad y_{c_2} = 0.1718, \qquad \varphi_2 = \frac{\pi}{3}$$

$$\text{Robot 3}: x_{c_3} = -0.3430, \qquad y_{c_3} = -0.5 \qquad \varphi_3 = \frac{\pi}{6}$$

Figs. 9, 10 and 11 illustrate errors of each robot with the RCC system. Besides, Fig. 12 represents the object tracking errors.

Desired and actual trajectories for robots 1, 2 and 3 and also the object (or the virtual structure) considering the model uncertainty are shown in Fig. 13.

In Fig. 14, the motion of the object along with the desired and real paths of the object have been presented. In Figs. 15–17, variations of some optimization factors, including load distribution among robots, path smoothness and system energy consumption for each robot, have been illustrated, respectively.

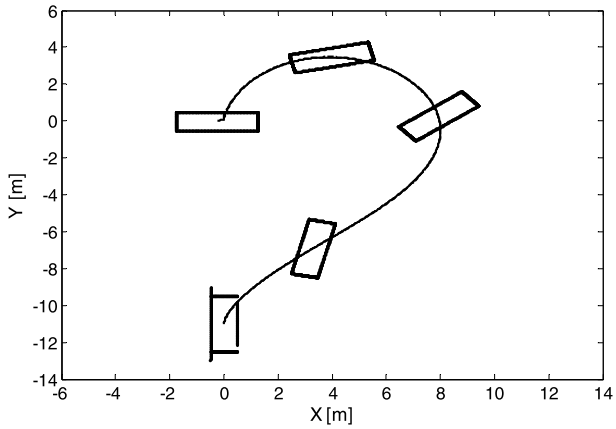

Fig. 14. Desired and real paths of the object along with its orientation.

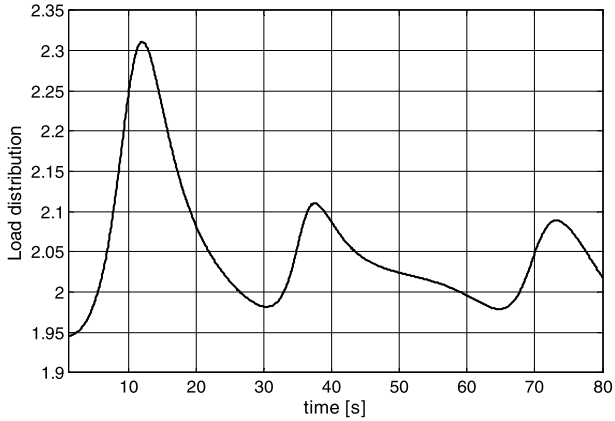

Fig. 15. Load distribution versus time.

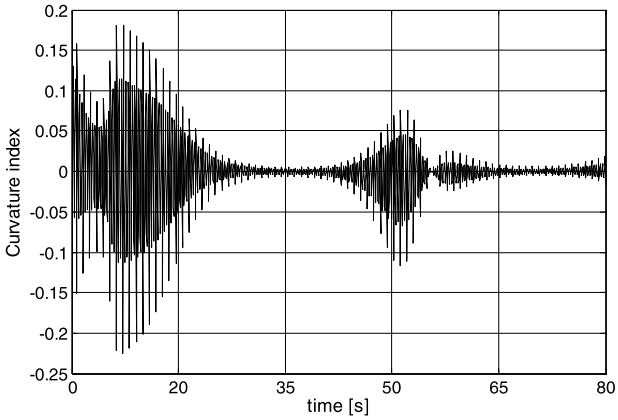

Fig. 16. Curvature effort.

As shown in Figs. 13 and 14, the object orientation starts from the initial value $\gamma = 0$ and once the robots move in the desired formation with pivot-grasp condition, the object orientation converges to a final value, $\gamma = 90$. As observed, imposing MIC law and exploiting RCC unit with robots in formation makes the errors converge to zero while the desired formation can be kept.

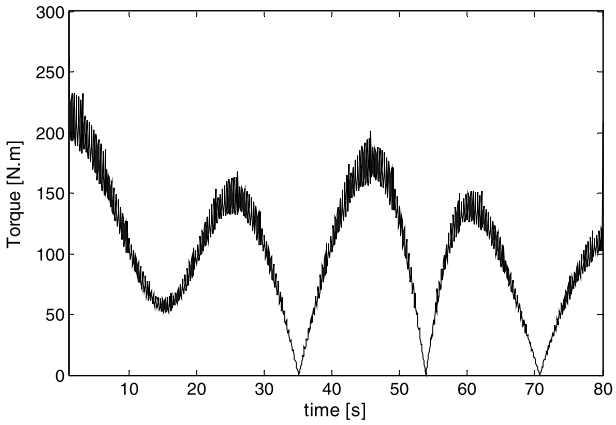

Fig. 17. Sum of torques of three robots.

7. Conclusions

Formation-based operations are crucial for many applications. However, the relative layouts of the team members within the formation can significantly affect the performance of team-based tasks. Hence, in this paper, we mainly investigated the creation of an optimized formation for members of a team of WMR moving in the plane. To solve the problem, a reasonable cost function has been considered, which includes control effort, load distribution among team members and path smoothness of the robots. Then, the positions of the grasping points were searched based on three numerical optimization approaches. The results show that in this problem, the minimum cost function value can be achieved using PSO approach. Furthermore, the MIC law was formulated and applied to the group of mobile robots. To examine the developed MIC law response, a system of three mobile robots manipulating a common object was simulated. The desired optimal formation was then tried to be kept using MIC control strategy with Remote Center Compliance (RCC) unit. Based on the simulation results, the merits of the MIC algorithm with RCC system in terms of robustness and tracking abilities were revealed, i.e. negligible small tracking errors can be achieved in the presence of significant uncertainty in the model parameters. This is due to the fact that based on the MIC law, all participating robots and the manipulated object exhibit the same impedance behavior, which guarantees an accordant motion of the various subsystems. The deep discussion on the employment of RCC and specially its active one along with MIC law for formation control will be the frame of future research by the authors.

References

[1] Shuang Liu, Dong Sun, Changan Zhu, Coordinated motion planning for multiple mobile robots along designed paths with formation requirement, IEEE/ASME Trans. Mechatron. 16 (6) (2011) 1021–1031.
[2] A. Abbaspour, S.A.A. Moosavian, K. Alipour, A virtual structure-based approach to formation control of cooperative wheeled mobile robots, in: First RSI/ISM International Conference on Robotics and Mechatronics, ICRoM 2013, Sharif University, Tehran, Iran, IEEE, 2013.
[3] W.A. Khan, C.P. Tang, V. Krovi, Modular and distributed forward dynamic simulation of constrained mechanical systems—a comparative study, Mech. Mach. Theory 42 (5) (2007) 558–579.
[4] Farbod Fahimi, Autonomous Robots, Modeling, Path Planning, and Control, Springer Science Business Media, LLC, 2009.
[5] Zhijun Li, Chenguang Yang, Yong Tang, Decentralised adaptive fuzzy control of coordinated multiple mobile manipulators interacting with non-rigid environments, IET Control Theory Appl. 7 (3) (2013) 397–410.
[6] Weiwei Shang, Shuang Cong, Yuan Ge, Coordination motion control in the task space for parallel manipulators with actuation redundancy, IEEE Trans. Autom. Sci. Eng. 10 (3) (2013) 605–673.
[7] V. Lippiello, B. Siciliano, L. Villani, A grasping force optimization algorithm for multi-arm robots with multi-fingered hands, IEEE Trans. Robot. 29 (1) (2013) 55–67.
[8] V. Lippiello, F. Ruggiero, B. Siciliano, L. Villani, Visual grasp planning for unknown objects using a multi-fingered robotic hand, IEEE/ASME Trans. Mechatron. 18 (3) (2013) 1050–1059.
[9] T. Niwa, S. Inagaki, T. Suzuki, Locomotion control of multi-legged robot based on follow-the-contact-point gait, in: ICCAS–SICE, 2009.
[10] M.H. Amoozgar, K. Alipour, S.H. Sadati, A fuzzy logic-based formation controller for wheeled mobile robots, Ind. Robot 38 (3) (2011) 269–281.
[11] A. Sadowskaa, T. van den Broekb, H. i Huijbertsa, N. van de Wouwc, D. Kostićc, H. Nijmeijerc, A virtual structure approach to formation control of unicycle mobile robots using mutual coupling, Int. J. Control 84 (11) (2011) 1886–1902.
[12] R.C. Arkin, Behavior-Based Robotics, MIT Press, London, 1998.
[13] P. Ogren, E. Fiorelli, N.E. Leonard, Formations with a mission: stable coordination of vehicle group maneuvers, in: Proc. International Symposium on Mathematical Theory of Networks and Systems, Notre Dame, IN, 2002.
[14] M. Bhatt, C.P. Tang, V.N. Krovi, Formation optimization for a fleet of wheeled mobile robots: a geometric approach, Robot. Auton. Syst. 57 (2009) 102–120.
[15] A. Hoskins, E. Atkins, Spacecraft formation optimization with a multi-impulse design, in: AIAA Guidance, Navigation and Control Conference and Exhibit, 2005.
[16] S.A.A. Moosavian, E. Papadopoulos, Cooperative object manipulation with contact impact using multiple impedance control, Int. J. Control. Autom. Syst. 8 (2) (2010) 314–327.
[17] R. Rastegari, S.A.A. Moosavian, Multiple impedance control of space free-flying robots via virtual linkages, Acta Astronaut. 66 (5–6) (2010) 748–759.

[18] K. Macek, Motion planning of mobile robots in indoor environments, M.Sc. thesis, University of Zagreb, Faculty of Electrical Engineering and Computing, Croatia, 2004.
[19] J. Kennedy, R. Eberhart, Particle swarm optimization, in: IEEE International Conference on Neural Networks, 1995, pp. 1942–1948.
[20] R.A. Rutenbar, Simulated annealing algorithms: an overview, Circuits Devices Mag. 5 (1) (1989) 19–26.
[21] H. Mesgari, F. Cheraghpour, S.A.A. Moosavian, Application of MAG index for optimal grasp planning, in: Proc. IEEE Int. Conf. on Mechatronics and Automation, Beijing, China, 2011.
[22] T.L. De Fazio, D.S. Seltzer, D.E. Whitney, The instrumented remote centre compliance, Ind. Robot 11 (4) (1984) 238–242.
[23] J.J. Craig, Introduction to Robotics: Mechanics and Control, 3rd ed., Pearson Education Inc. Upper Saddle River, NJ, USA, 2005.